Supporting Information for

Selective C-C Coupling in Carbon Dioxide Electroreduction via Efficient Spillover of Intermediates as Supported by Operando Raman Spectroscopy

Jing Gao[a,b], Hong Zhang[b], Xueyi Guo[a], Jingshan Luo[b,c], Shaik M. Zakeeruddin[b], Dan Ren[b,*], Michael Grätzel[b,*]

a. School of Metallurgy and Environment, Central South University, Changsha, 410083 Hunan, China
b. Laboratory of Photonics and Interfaces, École Polytechnique Fédérale de Lausanne, 1015 Lausanne, Switzerland
c Institute of Photoelectronic Thin Film Devices and Technology, Key Laboratory of Photoelectronic Thin Film Devices and Technology of Tianjin, College of Electronic Information and Optical Engineering, Nankai University, 300350 Tianjin, China

*Correspondence should be addressed to D.R. and M.G.: dan.ren@epfl.ch,

michael.graetzel@epfl.ch

Table of Contents

S1. Additional characterizations of $Cu(OH)_2$, Cu_2O and Cu_2O-Ag

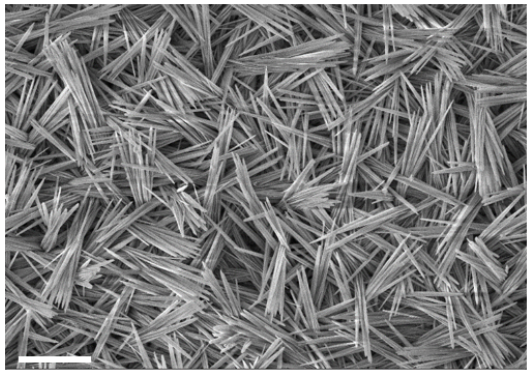

Figure S1 Scanning electron micrograph of as-prepared $Cu(OH)_2$ nanowires. Scale bar: 4 μm.

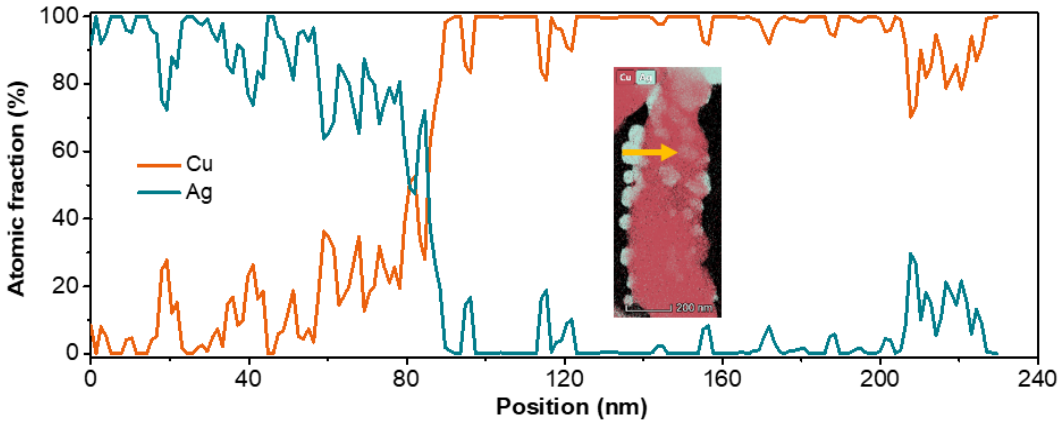

Figure S2 The elemental profiling of Cu and Ag on a representative Ag-Cu_2O nanowire (see insert) as a function of position. The arrow in inserted HAADF image shows the profiling direction.

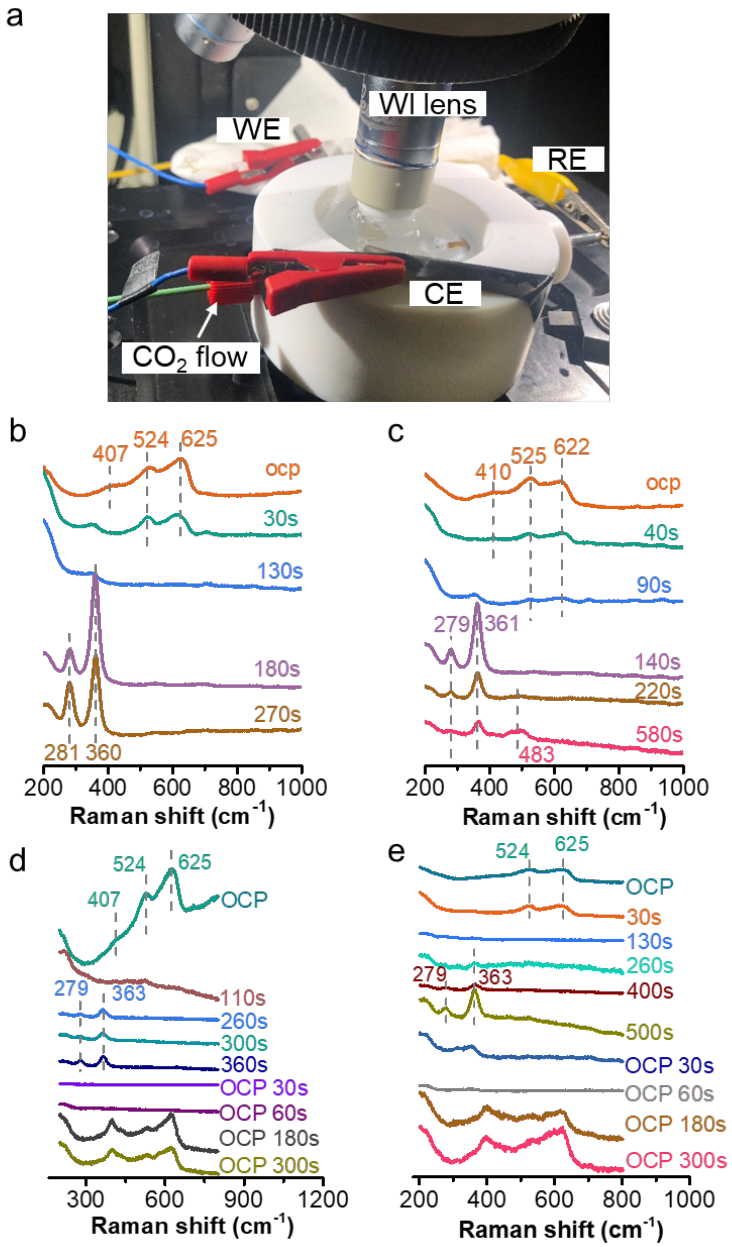

Figure S3 (a) A photograph of the custom-built electrochemical Teflon cell used for collecting operando Raman spectra during CO_2 reduction. CO_2 gas was continuously flowed through the cell during measurement. WE, CE, RE and WI lens refer to working electrode, counter electrode, reference electrode and water immersion lens, respectively. Operando Raman spectra of **(b, d)** Cu_2O and **(c, e)** Cu_2O-Ag during prereduction at -5 mA in 0.1 M $KHCO_3$. A near-infrared laser (785 nm) was used as the excitation source. Raman peaks located at 407-410, 524-525 and 622-625 cm^{-1} are assigned to the vibrations of Cu_2O.

S2. Characterizations of oxide-derived Cu and CuAg catalysts

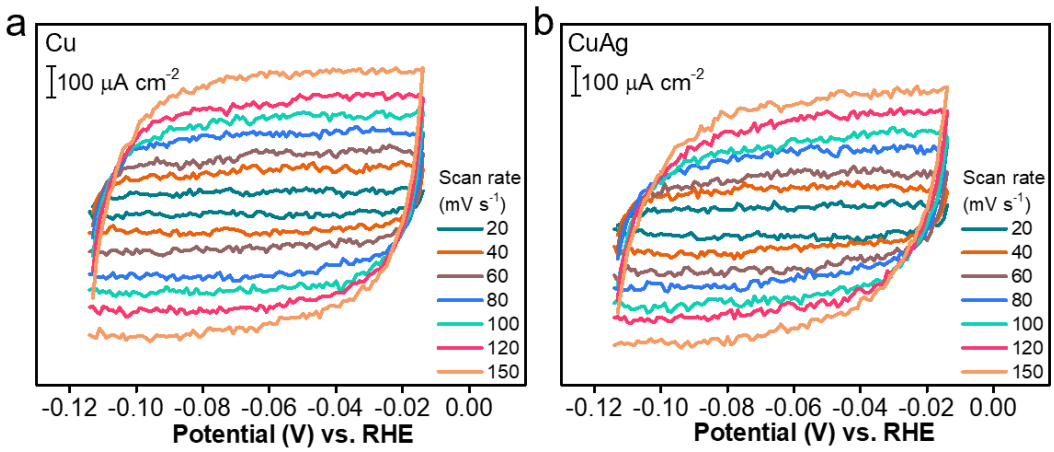

Figure S4 Representative cyclic voltammograms within a non-faradaic potential range of **(a)** Cu and **(b)** CuAg at different scant rates from 20 to 150 mV s^{-1} in Ar-saturated 0.1 M $KHCO_3$.

Table S1 The roughness factors of Cu and CuAg catalysts estimated from double layer capacitance.

Catalysts	Double layer capacitance (mF cm^{-2})	Roughness factor
Cu	3.40±0.44 [a]	113.3±14.7
CuAg	2.76±0.04	92.0±1.3

[a] The capacitance values of Cu and CuAg correspond to the average value of three independent measurements and the error bars are the standard deviations of these measurements.

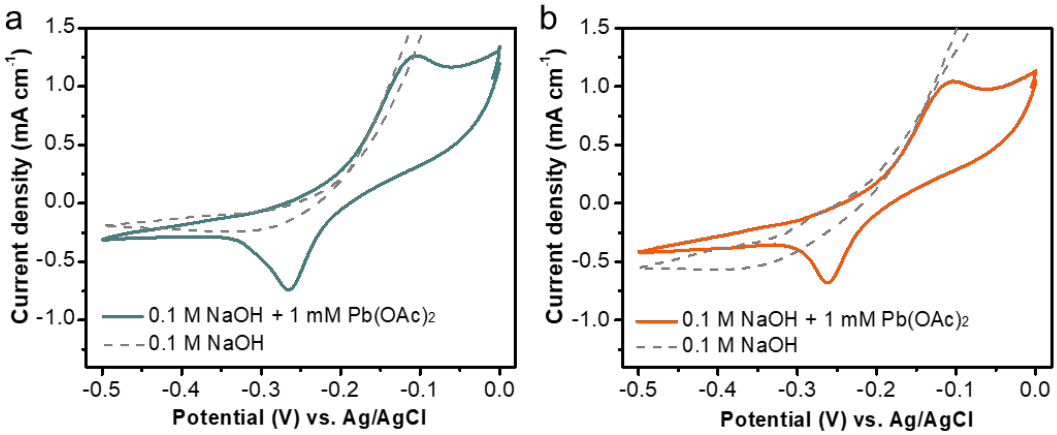

Figure S5 Representative cyclic voltammograms of Pb underpotential deposition on **(a)** Cu and **(b)** CuAg in 0.1 M NaOH + 1 mM $Pb(OAc)_2$ (solid line) and 0.1 M NaOH (dash line). Scan rate was 10 mV s^{-1}. The cathodic and anodic peaks observed at -0.27 V and -0.11 V correspond to the underpotential deposition of Pb and stripping of the Pb, respectively.

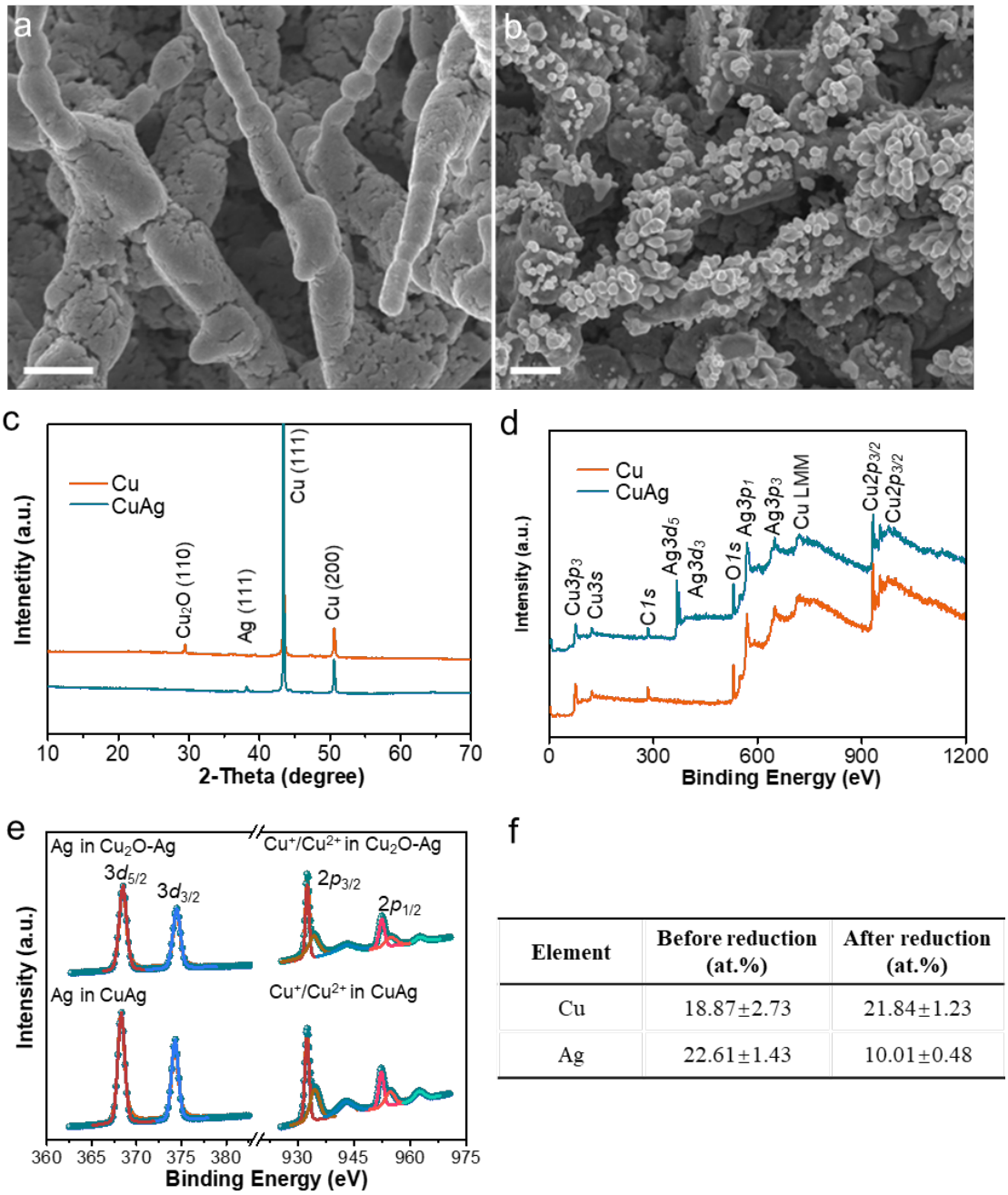

Element	Before reduction (at.%)	After reduction (at.%)
Cu	18.87±2.73	21.84±1.23
Ag	22.61±1.43	10.01±0.48

Figure S6 Morphological and chemical characterizations of Cu and CuAg after 60-min electrolysis. SEM images of **(a)** Cu and **(b)** CuAg electrodes after 60-min CO_2 electroreduction at -1.05 V. **(c)** X-ray diffractograms, **(d)** XPS survey spectra, and **(e)** high-resolution XPS spectra of Cu2p and Ag3d after 60-min CO_2 electroreduction at -1.05 V. **(f)** Atomic percentage of Cu and Ag at the surface of CuAg catalyst before and after 60-min CO_2 reduction (the rest corresponds to the oxygen and carbon). Scale bar: 500 nm for **(a)** and **(b)**.

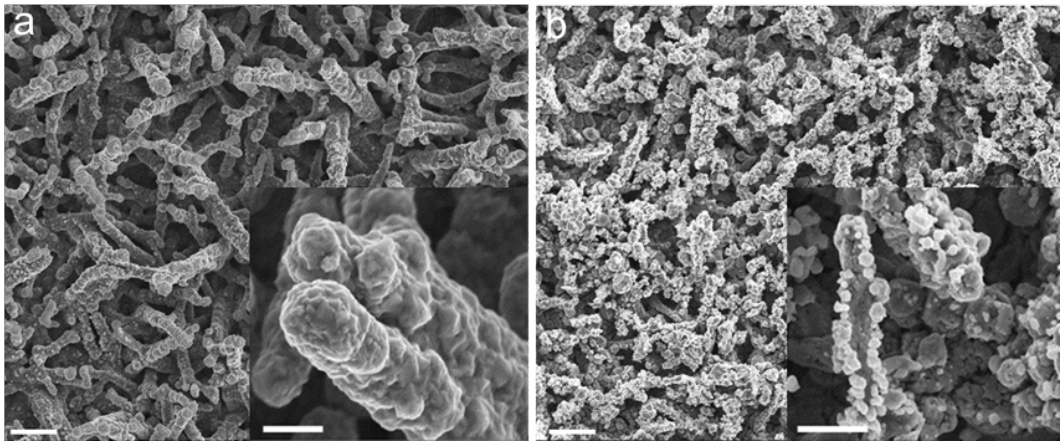

Figure S7 Scanning electron micrographs of **(a)** Cu and **(b)** CuAg after 12 h stability test. Scale bars: 2 μm for **(a)** and **(b)**, 500 nm for the inserts.

S3. Electrochemical reduction of carbon dioxide on Cu and CuAg

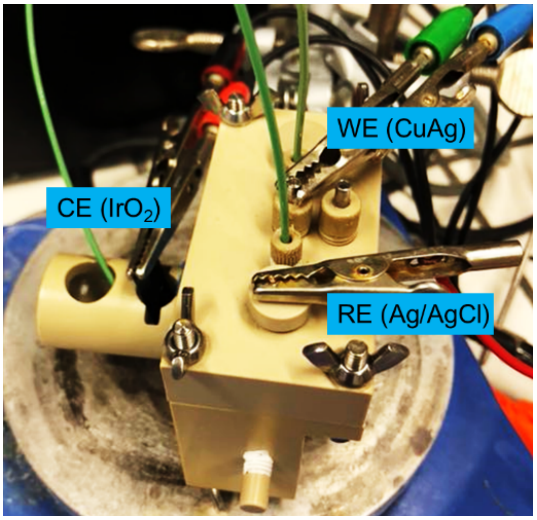

Figure S8 A photograph of the electrochemical peek cell used for CO_2 reduction experiments in this work. The custom-built cell is separated into two compartments by an anion exchange membrane. The working electrode (WE) is held in the airtight cathodic compartment, with the reference electrode (RE) placed nearby. CO_2 gas is infused into the cathodic and anodic compartments at the same flow rate of 10 mL min^{-1}.

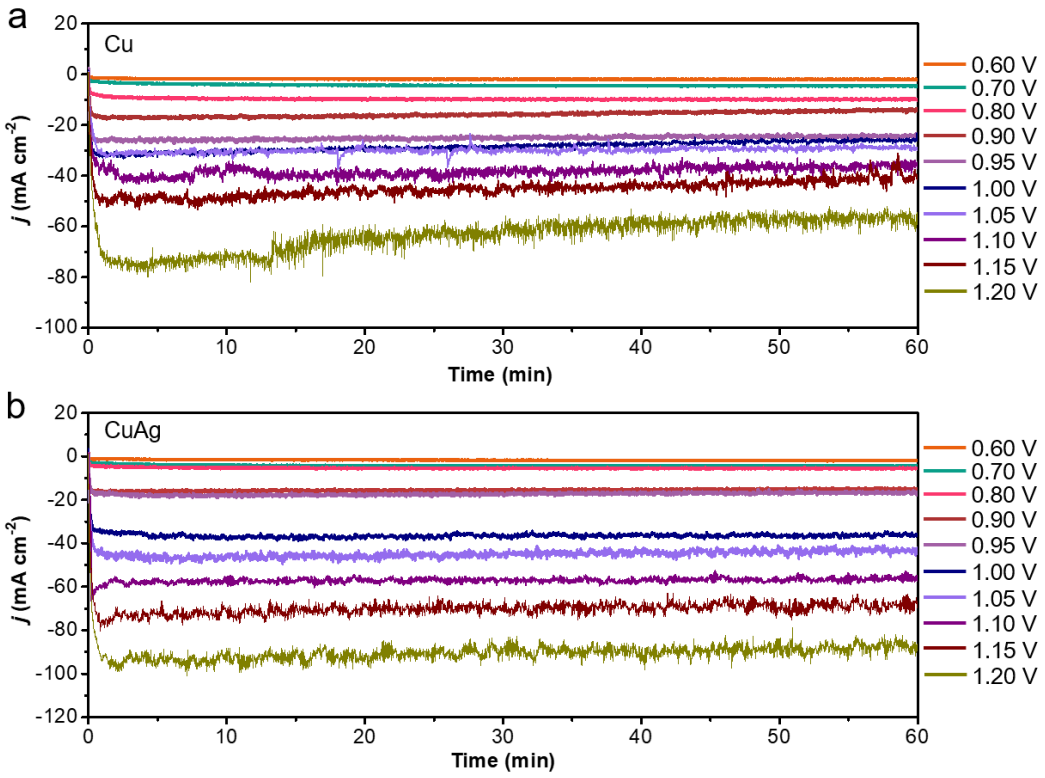

Figure S9 Representative chronoamperograms of **(a)** Cu and **(b)** CuAg cathodes over 60-min electrolysis at different potentials.

S4. Faradaic efficiency and partial current density for products

All the detected products during CO_2 reduction were expressed in terms of faradaic efficiency and partial current density. The FE of product *X* is defined as:

$$\mathrm{FE}(X) = \frac{\text{number of electrons used for producing } X \text{ from } \mathrm{CO_2}}{\text{total number of electrons for electrolysis}} \times 100\%$$

The partial current density of product *X* is defined as:

$$j(X) = \mathrm{FE}(X) \times j_{total}$$

To give an example for the calculation of faradaic efficiency, we listed a representative set of data recorded on a CuAg catalyst at -1.05 V in Table S2.

Table S2 Current and amounts of gaseous products recorded for five consecutive injections during 60-min electrolysis, and concentration of liquid products produced after the electrolysis.

vial	time (s)	*j* (mA)	amount (picomol)			concentration (μM)			
			H_2	CO	C_2H_4	$HCOO^-$	C_2H_5OH	C_3H_7OH	CH_3COH
1	-	-	-	-	-				
2	945	-9.84	748.60	20.93	234.54				
3	1790	-9.69	798.77	24.09	244.37	598.86	675.00	119.43	33.75
4	2635	-9.40	728.71	24.01	224.89				
5	3480	-9.47	726.66	28.71	219.22				

Gaseous products

The faradaic efficiency for each gaseous product is the average of the last four injections since the products in first injection were not equilibrated in the headspace. Here we calculate the faradaic efficiency of ethylene based on the data from vial 2 as an example.

12 electrons are required to form one ethylene molecule from two CO_2 molecules. Thus the number of electrons needed to get *x* (234.54) picomol of ethylene was:

$$n_{ethylene} = x \times N_A \times 12\mathrm{e} = 234.53 \times 10^{-12}\ \mathrm{mol} \times 6.02 \times 10^{23}\ \mathrm{mol^{-1}} \times 12\mathrm{e} = 1.69 \times 10^{15}\mathrm{e}$$

The flow rate of the CO_2 was set as 10 $cm^3\ min^{-1}$ (v_0). The pressure difference between the gas inlet and atmosphere (1 atm = 14.7 psi) was recorded as 1.9 psi. Hence

the actual flow rate at the gas outlet was:

$$v = \frac{P_0+\Delta P}{P_0} \times v_0 = \frac{(14.7+1.9)\ \text{psi}}{14.7\ \text{psi}} \times 10\ \text{cm}^3\ \text{min}^{-1} = 11.29\ \text{cm}^3\ \text{min}^{-1}$$

Thus, the total time required to fill up the sample loop (10 μL) was:

$$t = \frac{V_0}{v} = \frac{0.01\ \text{cm}^3}{11.29\ \text{cm}^3\ \text{min}^{-1}} = 0.00089\ \text{min} = 0.053\ \text{s}$$

The total number of electrons passed during the sampling of vial 2 was:

$$n_{total} = \frac{I_0 \times t}{e} = \frac{9.84\times10^{-3}\ \text{A}\times0.053\ \text{s}}{1.602\times10^{-19}\ \text{C e}^{-1}} = 3.26\times10^{15}\text{e}$$

Thus, the faradaic efficiency of ethylene in vial 2 was:

$$\text{FE} = \frac{n_{ethylene}}{n_{total}} \times 100\% = \frac{1.69\times10^{15}\text{e}}{3.26\times10^{15}\text{e}} \times 100\% = 51.8\%$$

Liquid products

Here we take the calculation of ethanol as an example. 12 electrons are required to form one ethanol molecule from two CO_2 molecules. Thus, the number of electrons required to produce 675.00 μM (c) ethanol in 8 mL (V) of catholyte was:

$$n_{ethanol} = c\times V\times N_A\times12\text{e} = 675\times10^{-6}\ \text{mol L}^{-1}\times8\times10^{-3}\ \text{L}\times6.02\times10^{23}\ \text{mol}^{-1}\times12\text{e} = 3.90\times10^{19}\text{e}$$

A total charge of 34.93 C (Q_0) was passed through over 60-min electrolysis. Hence, the total number of electrons passed during CO_2 reduction reaction was:

$$n_{total} = \frac{Q_0}{e} = \frac{34.93\ \text{C}}{1.602\times10^{-19}\ \text{C e}^{-1}} = 2.18\times10^{20}\text{e}$$

Thus, the faradaic efficiency of ethanol was:

$$\text{FE} = \frac{n_{ethanol}}{n_{total}} \times 100\% = \frac{3.90\times10^{19}\text{e}}{2.18\times10^{20}\text{e}} \times 100\% = 17.9\%$$

The sum of all FE values remained in the range of 90-105% (Table S5-S6), indicating that our experimental protocol is comprehensive and the instruments are well calibrated[1].

Table S3 Average current densities of products from CO_2 reduction on Cu_2O derived Cu catalyst at different potentials.

Potential (V) vs. RHE	H_2	CO	CH_4	$HCOO^-$	C_2H_4	C_2H_5OH	CH_3COO^-	CH_3COH	C_3H_7OH
-0.60	1.35	0.15	-	0.71	-	-	-	-	-
-0.70	1.75	0.29	-	1.76	0.07	-	-	-	-
-0.80	4.59	0.47	-	3.15	0.39	0.08	-	-	0.10
-0.90	4.85	0.48	-	4.44	1.37	0.47	0.05	-	0.60
-0.95	7.23	0.42	0.17	2.69	4.67	1.73	0.08	0.11	1.59
-1.00	7.98	0.29	0.70	2.54	8.36	3.28	0.12	0.25	1.83
-1.05	9.33	0.16	0.50	0.72	8.53	4.64	0.10	0.16	1.77
-1.10	14.08	0.18	2.02	0.54	8.98	5.38	0.07	0.21	1.45
-1.15	27.3	0.31	5.86	0.43	12.84	5.74	0.08	0.25	1.43
-1.20	42.13	0.21	8.88	0.55	7.83	3.99	0.11	0.24	1.17

Table S4 Average current densities of products from CO_2 reduction on Cu_2O derived CuAg catalyst at different potentials.

Potential (V) vs. RHE	H_2	CO	CH_4	$HCOO^-$	C_2H_4	C_2H_5OH	CH_3COO^-	CH_3COH	C_3H_7OH
-0.6	1.01	0.18	-	0.46	0.04			-	-
-0.7	1.88	0.43	-	1.16	0.03			-	-
-0.8	2.63	0.70	-	1.93	0.21	0.13	-	-	0.21
-0.9	5.36	1.24	-	2.30	1.71	0.58	0.07	0.12	0.90
-0.95	6.47	1.49	-	1.55	4.39	1.62	0.11	0.17	1.83
-1.0	6.93	0.69	-	1.42	9.59	4.22	0.13	0.34	2.25
-1.05	8.54	0.41	-	0.92	18.07	6.07	0.11	0.38	2.12
-1.1	21.61	0.31	0.80	0.58	16.88	6.37	0.09	0.25	1.64
-1.15	31.85	0.42	3.30	0.53	17.09	7.66	0.12	0.37	1.74
-1.2	50.40	0.49	5.48	0.48	12.50	6.30	0.08	0.31	1.23

Table S5 Average faradaic efficiencies of products from CO_2 reduction on Cu_2O derived Cu catalyst at different potentials.

Potential (V) vs. RHE	H_2	CO	CH_4	$HCOO^-$	C_2H_4	C_2H_5OH	CH_3COO^-	CH_3COH	C_3H_7OH	FE_{total}	j_{total}	$j_{specific}$
-0.6	59.93	.83	-	32.97	N.D.	N.D.	N.D.	N.D.	N.D.	99.73	2.23	0.02
-0.7	44.77	.07		43.77	1.80	N.D.	N.D.	N.D.	N.D.	97.41	3.95	0.03
-0.8	50.80	.20	N.D.	34.50	4.17	0.93	N.D.	N.D.	1.20	96.80	9.13	0.08
-0.9	38.43	.60	N.D.	33.83	10.80	3.87	0.35	0.65	4.70	96.23	12.85	0.11
-0.95	39.70	.23	0.90	15.20	23.83	8.63	0.43	0.53	8.17	99.62	19.0	0.17
-1	31.33	.13	2.50	9.50	33.20	13.10	0.43	0.93	7.20	99.32	25.47	0.22
-1.05	34.93	.53	1.60	2.53	30.47	16.43	0.33	0.75	5.43	93.00	28.08	0.25
-1.1	41.97	.50	5.47	1.53	25.47	15.13	0.20	0.57	3.90	94.74	35.20	0.31
-1.15	50.10	.60	10.30	0.80	24.07	10.57	0.17	0.43	2.60	99.64	54.43	0.48
-1.2	60.03	.37	12.37	0.80	12.13	6.23	0.30	0.37	1.80	94.40	68.94	0.61

The data is partially from Ref 1.

Table S6 Average faradaic efficiencies of products from CO_2 reduction on Cu_2O derived CuAg catalyst at different potentials.

Potential (V) vs. RHE	H_2	CO	CH_4	$HCOO^-$	C_2H_4	C_2H_5OH	CH_3COO^-	CH_3COH	C_3H_7OH	FE_{total}	j_{toal}	$j_{specific}$
-0.6	55.40	10.10	N.D.[a]	25.27	0.57	N.D.	N.D.	N.D.	N.D.	91.34	1.82	0.02
-0.7	51.40	11.47	N.D.	31.77	0.93	N.D.	N.D.	N.D.	N.D.	95.57	3.69	0.04
-0.8	42.13	11.77	N.D.	31.30	3.30	2.23	N.D.	N.D.	3.47	94.20	6.20	0.07
-0.9	41.40	10.23	N.D.	18.47	12.93	4.53	0.53	1.00	6.83	95.92	12.66	0.14
-0.95	35.23	7.70	N.D.	8.50	24.00	8.80	0.57	0.90	9.80	95.50	18.62	0.20
-1	24.40	2.23	N.D.	4.90	34.03	14.90	0.43	1.20	7.97	90.06	28.58	0.31
-1.05	25.50	1.07	N.D.	2.57	51.50	17.50	0.30	1.00	5.63	105.07	35.12	0.38
-1.1	45.13	0.63	1.67	1.23	35.33	13.13	0.25	0.50	3.33	101.20	48.04	0.52
-1.15	50.27	0.63	5.13	0.80	26.13	11.73	0.17	0.57	2.67	98.10	64.43	0.70
-1.2	62.90	0.63	7.03	0.63	15.70	7.87	0.10	0.40	1.53	96.79	80.29	0.87

Table S7 The performances of Cu-based catalysts for the electroreduction of CO_2 to ethylene.

Catalyst	Electrolyte	Applied potential/current density	Performance towards ethylene formation		
			Faradaic efficiency (%)	Current density (mA cm^{-2})	Specific current density (mA cm^{-2})
polycrystalline Cu[2]	0.1 M $KHCO_3$	-1.41 V vs. NHE[a]	30.1	-1.5	-1.5
	0.1 M $KClO_4$	-1.40 V vs. NHE	48.1	-2.4	-2.4
	0.1 M KCl	-1.44 V vs. NHE	47.8	-2.4	-2.4
	0.1 M K_2SO_4	-1.40 V vs. NHE	46.0	-2.3	-2.3
Cu (100)[3]	0.1 M $KHCO_3$	-1.40 V vs. SHE[b]	40.4	-2.0	-2.0
Cu (911)[3]	0.1 M $KHCO_3$	-1.36 V vs. SHE	50.9	-2.6	-2.6
Cu (711)[3]	0.1 M $KHCO_3$	-1.34 V vs. SHE	50.0	-1.5	-1.5
Cu nanocrystals[4]	0.1 M $KHCO_3$	-1.10 V vs. RHE	41.1	-1.2	-1.7
Cu nanoparticles (using flow cell)[5]	1 M KOH	-0.79 V vs. RHE	45.6	-138.0	-115
1.7 μm Cu_2O[6]	0.1 M $KHCO_3$	-0.99 V vs. RHE	38.8	-11.6	-2.5
Cu_2O derived Cu[7]	0.1 M $KHCO_3$	-31.2 mA cm^{-2}	42.6	-13.3	-0.1
Ag@Cu[8]	0.1 M $KHCO_3$	-1.06 V vs. RHE	28.6	-1.1	N.R.
Cu/Ag[9]	0.2 M $CsHCO_3$	-1.0 V vs. RHE	22.0	~-2.2	N.R.
Ag-Cu_2O_{PS}[10]	0.2 M KCl	-1.3 V vs. RHE	11.0	-0.3	N.R.
Ag-Cu_2O_{PB}[10]	0.2 M KCl	-1.2 V vs. RHE	9.5	-0.3	N.R.
CuAg wire (using flow cell)[11]	1 M KOH	-0.7 V vs. RHE	55.0	-180.0	-22.2
CuAu[12]	0.1 M $KHCO_3$	-1.05 V vs. RHE	38.7	-16.6	-1.7
7.9 μm CuBr[13]	3 M KBr	-2.4 V vs. Ag/AgCl	79.5	-36.0	N.R.[c]
CuAg (this work)	0.1 M $KHCO_3$	-1.0 V vs. RHE	51.5	-18.1	-1.6

[a] NHE: normal hydrogen electrode; [b] SHE: standard hydrogen electrode; [c] N.R.: not reported

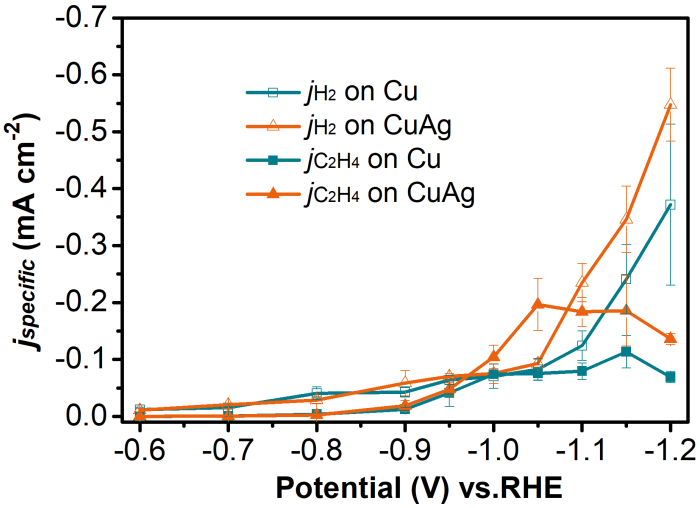

Figure S10 Specific current densities of hydrogen (j_{H_2}) and ethylene ($j_{C_2H_4}$) as a function of applied potential on Cu and CuAg catalysts.

S5. CO_2 reduction on Ag nanocorals

Preparation of Ag nanocorals

1-μm-thick Ag was sputtered onto etched FTO glass (DP650, Alliance-Concept), followed by anodization in 0.1 M Ar-saturated KCl solution (99.5% metal basis, Sigma Aldrich) at 0.4 V vs. RHE for 2 min to form a grey film[14]. The resulting film was then pre reduced in 0.1 M CO_2-saturated $KHCO_3$ (99.99% metal base, Sigma Aldrich) solution at -1.8 V vs. RHE for 2 min.

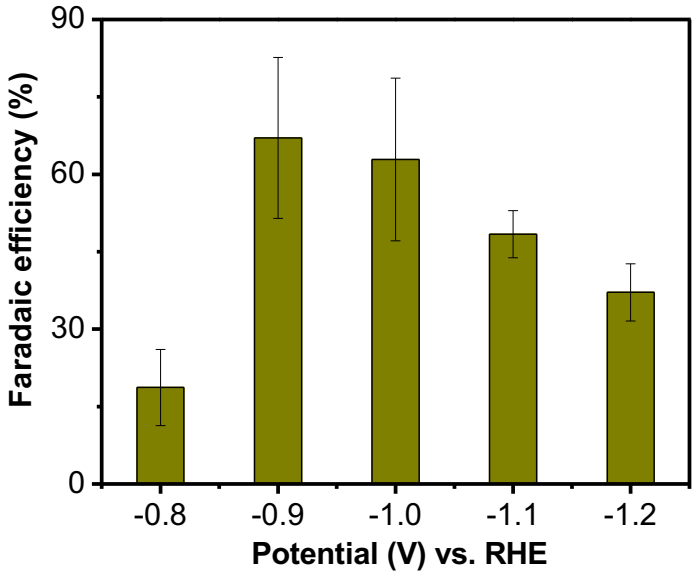

Figure S11 Faradaic efficiency of CO as a function of applied potential on pure Ag nanocorals.

S6. CO_2 reduction on planar Cu_2O-Ag

Preparation of planar Ag-Cu_2O

Planar Cu_2O was prepared by electrochemical deposition method adapted from a previous work[6]. Briefly, Cu film with thickness of 200 nm was sputtered on the surface of etched FTO (TEC-15 Ω), which was used as the deposition substrate. Cu_2O film was electrochemically deposited onto the substrate from 0.3 M $CuSO_4$ electrolyte containing 2.3 M lactic acid and 3.2 M NaOH, which was kept at 60 °C in a water bath. The deposition was carried out at a constant current density of -1.82 mA cm^{-2} for 10 min. The resulting Cu_2O film was then soaked into 10 mM $AgNO_3$ solution for 5 min to form planar Ag-Cu_2O.

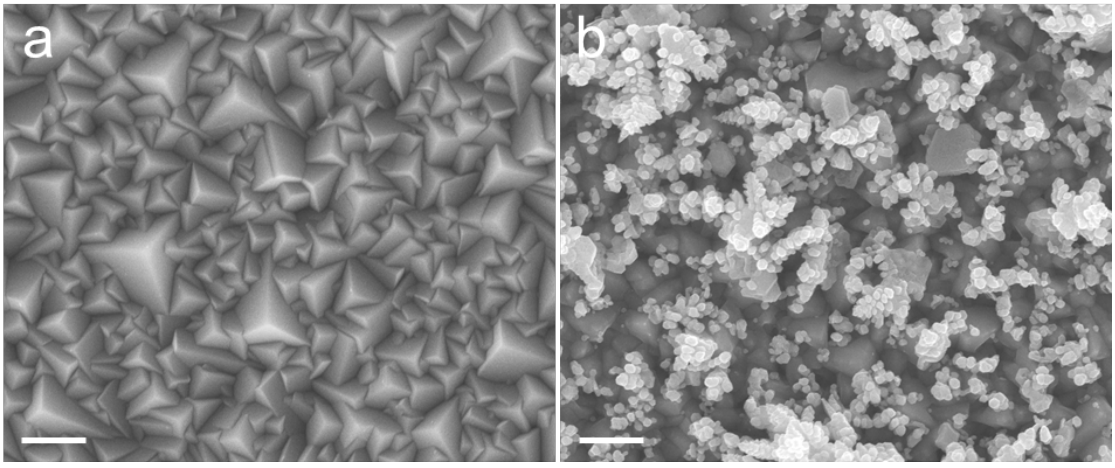

Figure S12 Scanning electron micrographs of **(a)** electrodeposited Cu_2O film and **(b)** exchanged Ag nanoparticles on Cu_2O film. Scale bars: 500 nm for **(a)** and **(b)**.

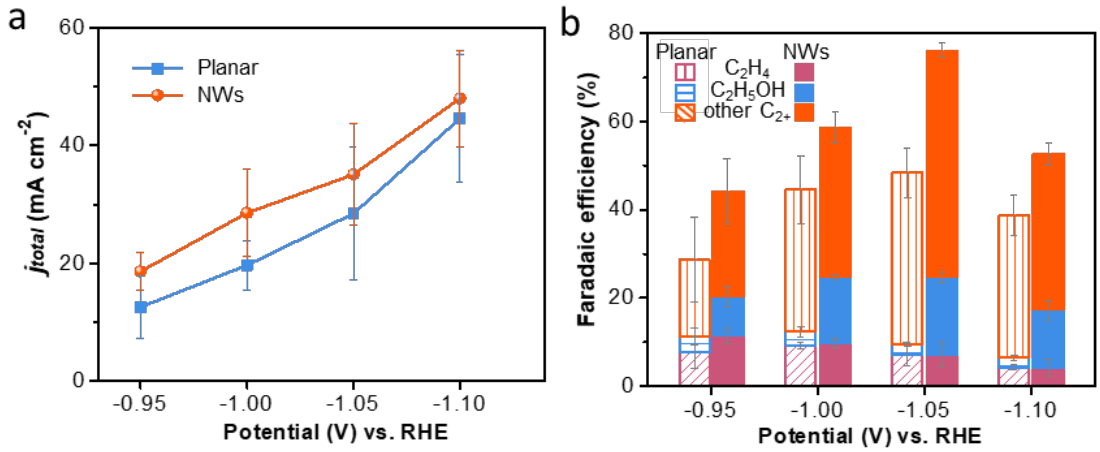

Figure S13 Comparison of performance on planar Cu_2O and Cu_2O NWs derived CuAg catalysts. **(a)** Total current density as a function of applied potential on planar Cu_2O and Cu_2O NWs derived CuAg catalysts. (b) Faradaic efficiencies of ethylene, ethanol and other C_{2+} products as a function of applied potential on planar Cu_2O and Cu_2O NWs derived CuAg catalysts.

S7. Raman spectroscopic studies on Ag

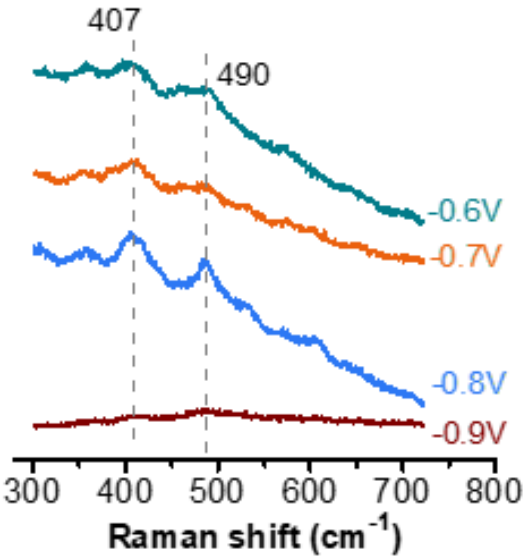

Figure S14 Operando Raman spectra of pure Ag at different potentials in 0.1 M $KHCO_3$. CO_2 was continuously flowed to the electrolyte and near-infrared laser (785 nm) was used as the excitation source. Raman peaks located at 407 and 490 cm^{-1} correspond to the CO vibration on Ag surface.

S8. SERS effect of Ag nanoparticles on Cu_2O

Preparation of Cu_2O on SERS substrate

1-μm-thick Ag was sputtered onto etched FTO glass (DP650, Alliance-Concept), followed by roughening in 0.1 M HCl (36%, ABCR) *via* cyclic voltammetry from -0.3 V to 0.2 V vs. Ag/AgCl. The prepared Ag nanoparticles was rinsed with DI water and dried by compressed air. Cu_2O was electrodeposited on the Ag surface using the same method as described above., except that the deposition time was 30 s.

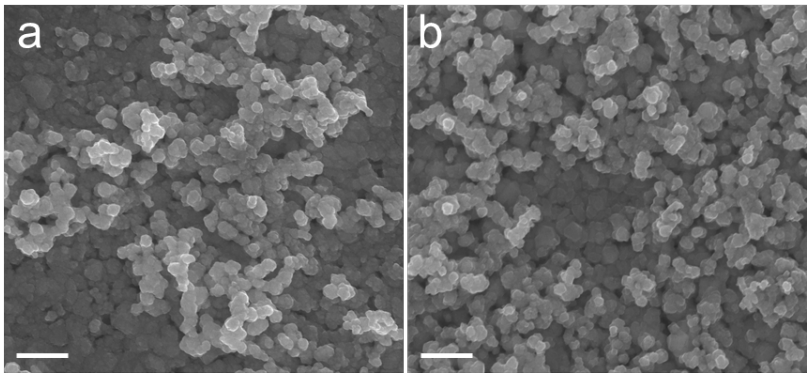

Figure S15 Scanning electron micrographs of **(a)** electrochemically-roughened Ag substrate and **(b)** electrodeposited Cu_2O on Ag substrate. Scale bars: 500 nm for **(a)** and **(b)**.

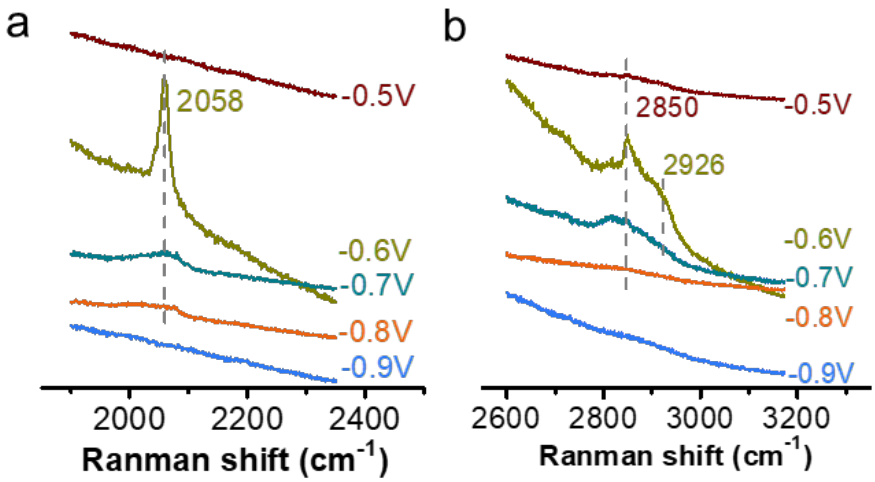

Figure S16 Operando Raman spectra of oxide-derived Cu onto a classic Ag SERS substrate. CO_2 was continuously flowed to 0.1 M $KHCO_3$ electrolyte and near-infrared laser (785 nm) was used as the excitation source. Raman peaks located at 2058 and 2850-2926 cm^{-1} correspond to the respective C≡O stretching and C-H vibration on Cu surface.

S9. Calculation of CO spillover efficiency

Calculation of turnover frequency (TOF)

The total production rate of CO (TOF_{CO}) was calculated against the specific surface area to analyze the efficiency of CO spillover on bimetallic catalysts. Generally, the produced CO from CO_2 electrochemical reduction exists in two forms: intermediated *CO and gaseous CO. The relationship between three terms is:

$$TOF_{CO} = TOF_{*CO} + TOF_{CO(g)}$$

We assume that all the hydrocarbons and oxygenates originate from *CO intermediates. Therefore, the production rate of *CO intermediates (TOF_{*CO}) can be calculated by equivalently converting the production rates of all the carbonaceous products via the following equation:

$$TOF_{*CO} = TOF_{CH_4} + 2TOF_{C_2H_4} + 2TOF_{C_2H_5OH} + 2TOF_{CH_3COO^-} + 2TOF_{CH_3COH} + 3TOF_{C_3H_7OH}$$

The difference of TOF_{CO} between Cu and CuAg is calculated to be the amount of CO produced on Ag active sites, defined here as ΔTOF_{CO}. The efficiency of CO spillover is thus expressed in the following equation:

$$\text{CO spillover efficiency} = \frac{\Delta TOF_{*CO}}{\Delta TOF_{CO}} = 1 - \frac{\Delta TOF_{CO(g)}}{\Delta TOF_{CO}}$$

It is noted that CO spillover only takes place at potentials <-1.0 V and is not applicable to more positive potentials.

Table S8 Calculated TOF values on Cu and CuAg with respect to specific surface area. CO spillover is supposed to take place only at potentials that are <-1.0 V.

Potential (V) vs. RHE	TOF_{CO} on Cu (nmol s^{-1} cm^{-2})	Standard error	TOF_{CO} on CuAg (nmol s^{-1} cm^{-2})	Standard error	$TOF_{CO(g)}$ on Cu (nmol s^{-1} cm^{-2})	Standard error	$TOF_{CO(g)}$ on CuAg (nmol s^{-1} cm^{-2})	Standard error	CO spillover efficiency	Propagated error
-0.6	0.71	0.26	1.03	0.17	0.71	0.24	1.03	0.17		
-0.7	1.41	0.44	2.50	0.51	1.32	0.42	2.39	0.51		
-0.8	2.91	1.06	4.67	0.96	2.12	0.79	4.02	1.20		
-0.9	5.38	0.97	12.07	0.39	2.21	1.06	6.96	1.74		
-0.95	14.56	7.06	23.80	5.87	1.94	1.15	8.37	5.98		
-1.0	22.77	1.59	35.22	8.91	1.32	0.50	3.91	2.61	0.79	0.26
-1.05	24.18	6.35	52.61	15.33	0.73	0.55	2.28	1.74	0.95	0.07
-1.1	27.80	7.94	50.43	9.67	0.85	0.57	1.74	0.73	0.96	0.05
-1.15	39.19	10.06	57.72	15.76	1.36	0.97	2.28	0.66	0.95	0.08
-1.2	31.77	4.32	48.70	2.28	1.06	0.65	2.83	0.67	0.90	0.06

S10. CO_2 reduction on CuAu

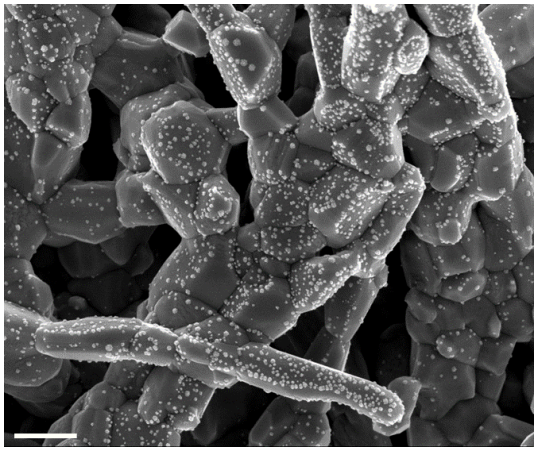

Figure S17 Scanning electron micrograph of Cu_2O-Au by driving galvanic replacement reaction between Cu_2O and $HAuCl_4$ (0.2 mM) for 1 min. Scale bar: 500 nm.

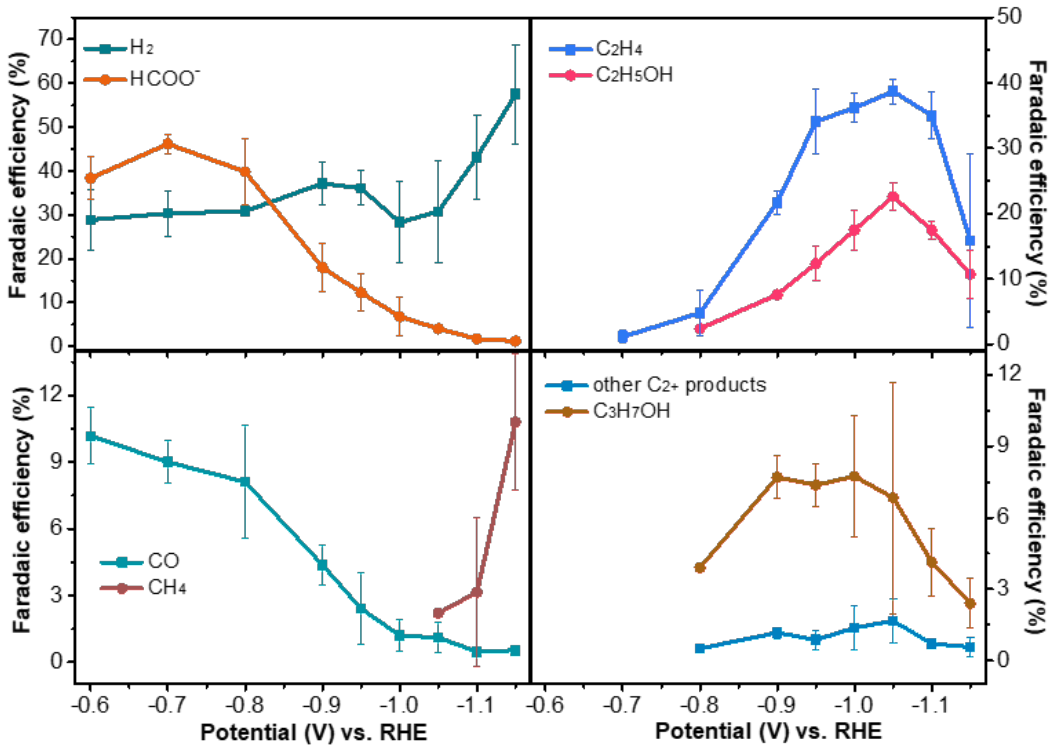

Figure S18 Faradaic efficiency for representative products on CuAu catalyst as a function of potential.

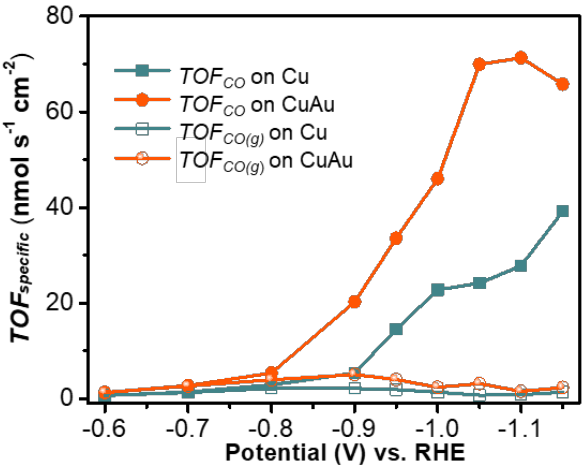

Figure S19 Production rates of total CO (including *CO intermediates and gaseous CO) and gaseous CO as a function of the applied potential on Cu and CuAu catalysts.

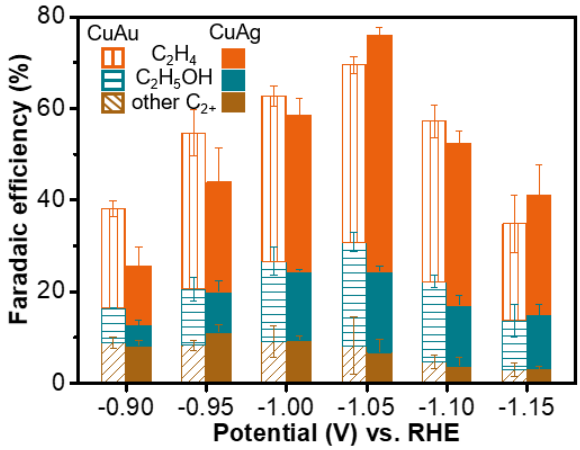

Figure S20 Average faradaic efficiencies of ethylene, ethanol and other C_{2+} products on CuAu (hollow) and CuAg (solid) catalysts. Data is obtained from Supporting Reference 12.

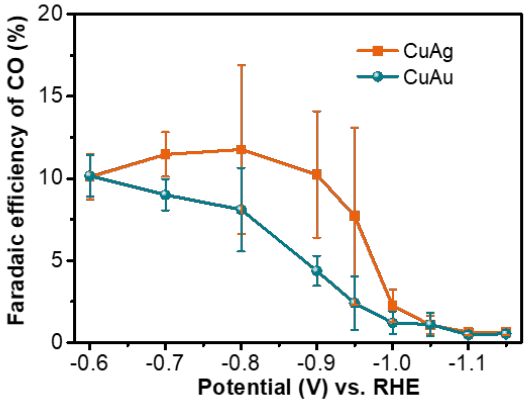

Figure S21 Faradaic efficiency of CO as a function of applied potential on CuAg and CuAu catalysts. Data is obtained from Supporting Reference 12.

S11 Solar-driven CO_2 reduction

Calculation of solar-to-fuel (STF) conversion efficiency

The STF conversion efficiency can be determined directly by the multiplier of electricity to fuel (ETF) output and solar to electricity (STE) input. For the CO_2 reduction system, STE and ETF conversion efficiency can be calculated respectively:

$$\eta_{STE} = \frac{electrtrical\ power\ output}{solar\ illumination\ input} = \frac{j_{op}V_{op}}{P_s}$$

$$\eta_{ETF} = \frac{fuel\ power\ output}{electrtrical\ power\ input} = \frac{j_{op}E_{fuel}FE_{fuel}}{j_{op}V_{op}}$$

Where j_{op} and V_{op} are the operating current and voltage of the combined system, Ps is the solar illumination input power, E_{fuel} is the thermodynamic equilibrium potential between the two half-reactions under standard condition and FE_{fuel} is the faradaic efficiency of the product. Thus, STF conversion efficiency can be calculated:

$$\eta_{STE} = \frac{\eta_{ETF}}{\eta_{STE}} = \frac{j_{op}E_{fuel}FE_{fuel}}{P_s}$$

An example of solar to ethylene conversion efficiency calculation is given here. The operating current density (normalized to the effective illuminated area of the solar cells) of the solar driven CO_2 reduction system is 6.68 mA cm^{-2}. The equilibrium cell potential for ethylene formation is 1.15 V. The average faradaic efficiency for ethylene formation was 54.26% during 1 h solar driven CO_2 reduction. The solar-to-ethylene conversion efficiency is calculated as:

$$\eta_{solar\text{-}to\text{-}ethylene} = \frac{6.68\ mA\ cm^{-2} \times 1.15\ V \times 54.26\%}{100\ mW\ cm^{-2}} = 4.17\%$$

Table S9 A summary of photovoltaic-driven electrochemical CO_2 reduction system from carbon dioxide and water.

Photovoltaic	Cathode	Anode	Electrolyte	Anolyte	Major product	Solar-to-fuel efficiency (%)	Ref.
GaInP/GaInAs/Ge	CuO + SnO_2	IrO_2	0.1 M $CsHCO_3$	0.25 CsOH	CO	13.4	[15]
Perovskite solar cell	Au	IrO_2	0.5 M $NaHCO_3$	-	CO	6.5	[16]
Si	WSe_2	Co	50% EMIM-BF4 in water	0.26 mM K^+	CO	4.6	[17]
GaAs/InGaP/Si	Pd/C coated Ti	Ni	2.8 M $KHCO3_3$	1 M KOH	HCOOH	10.0	[18]
SiGe	Ru complex polymer	IrO_x	0.1 M potassium phosphate buffer (K_2HPO_4:KH_2PO_4 = 1:1)	-	HCOOH	4.6	[19]
Si	Cu_2O derived Cu	IrO_x	0.2 M $KHCO_3$	-	C_2H_4	1.5	[20]
III-V/Si	CuAg	IrO_2	0.2 M $CsHCO_3$	0.2 M $CsHCO_3$	C_2H_4	1.7	[9]
Perovskite solar cell	CuO	CuO	0.1 M $CsHCO_3$	0.2 M Cs_2CO_3	C_2H_4+C_2H_6	2.3	[21]
Perovskite solar cell	CuAg	IrO_2	0.2 M $KHCO_3$	-	C_2H_4	4.2	this work

Table S10 Faradaic efficiencies of products obtained from CO_2 reduction on Cu_2O derived CuAg catalyst at different current densities in two-electrode configuration.

Current density (mA cm^{-2})	H_2	CO	$HCOO^-$	C_2H_4	C_2H_5OH	C_3H_7OH	FE_{total}
30.30	21.66	3.05	7.0	35.48	22.1	4.20	93.5
35.29	26.09	1.30	7.6	42.41	7.3	0.9	85.6
40.70	32.82	0.80	4.18	52.94	11.3	2.3	104.9
43.38	32.80	0.76	5.1	51.92	10.6	2.7	103.9
46.84	37.00	0.59	7.1	49.98	7.40	2.1	104.2
52.30	27.76	0.44	2.30	50.74	12.50	2.20	96.0
56.94	28.68	0.89	2.9	52.26	7.80	3.10	92.0

Table S11 Overall reaction for the major products and the respective energy efficiency of solar-driven electrolyzer system.

Reduction product	Overall reaction	Equilibrium potential (V)	Faradaic efficiency (%)	Solar to fuel conversion efficiency (%)
hydrogen	$2H_2O \rightarrow 2H_2 + O_2$	1.23	22.6	1.86
carbon monoxide	$2CO_2 \rightarrow 2CO + O_2$	1.33	0.66	0.06
formate	$2CO_2 + 2H_2O \rightarrow 2HCOO^- + 2H^+ + O_2$	1.46	3.70	0.31
acetate	$2CO_2 + 2H_2O \rightarrow CH_3COO^- + H^+ + 2O_2$	1.15	0.30	0.03
ethylene	$2CO_2 + 2H_2O \rightarrow C_2H_4 + 3O_2$	1.15	54.26	4.17
ethanol	$2CO_2 + 3H_2O \rightarrow C_2H_5OH + 3O_2$	1.14	13.10	1.00
n-propanol	$6CO_2 + 8H_2O \rightarrow 2C_3H_7OH + 9O_2$	1.02	3.70	0.25
acetone	$3CO_2 + 3H_2O \rightarrow CH_3COCH_3 + 4O_2$	1.37	1.10	0.10

S12. Supporting References

1. Hori, Y., Electrochemical CO_2 Reduction on Metal Electrodes. In *Modern Aspects of Electrochemistry*, Vayenas, C. G.; White, R. E.; Gamboa-Aldeco, M. E., Eds. Springer New York: 2008; Vol. 42, pp 89-189.
2. Hori, Y.; Murata, A.; Takahashi, R., Formation of Hydrocarbons in the Electrochemical Reduction of Carbon Dioxide at a Copper Electrode in Aqueous Solution. *J. Chem. Soc., Faraday Trans. 1* **1989,** *85* (8), 2309-2326.
3. Hori, Y.; Takahashi, I.; Koga, O.; Hoshi, N., Electrochemical Reduction of Carbon Dioxide at Various Series of Copper Single Crystal Electrodes. *J. Mol. Catal. A: Chem.* **2003,** *199* (1–2), 39-47.
4. Loiudice, A.; Lobaccaro, P.; Kamali, E. A.; Thao, T.; Huang, B. H.; Ager, J. W.; Buonsanti, R., Tailoring Copper Nanocrystals towards C_2 Products in Electrochemical CO_2 Reduction. *Angew. Chem. Int. Ed.* **2016,** *55* (19), 5789-5792.
5. Ma, S.; Sadakiyo, M.; Luo, R.; Heima, M.; Yamauchi, M.; Kenis, P. J. A., One-step electrosynthesis of ethylene and ethanol from CO_2 in an alkaline electrolyzer. *J. Power Sources* **2016,** *301*, 219-228.
6. Ren, D.; Deng, Y.; Handoko, A. D.; Chen, C. S.; Malkhandi, S.; Yeo, B. S., Selective Electrochemical Reduction of Carbon Dioxide to Ethylene and Ethanol on Copper(I) Oxide Catalysts. *ACS Catal.* **2015,** *5* (5), 2814-2821.
7. Handoko, A. D.; Ong, C. W.; Huang, Y.; Lee, Z. G.; Lin, L.; Panetti, G. B.; Yeo, B. S., Mechanistic Insights into the Selective Electroreduction of Carbon Dioxide to Ethylene on Cu_2O-Derived Copper Catalysts. *J. Phys. Chem. C* **2016,** *120* (36), 20058-20067.
8. Chang, Z.; Huo, S.; Zhang, W.; Fang, J.; Wang, H., The tunable and highly selective reduction products on Ag@Cu bimetallic catalysts toward CO_2 electrochemical reduction reaction. *J. Phys. Chem. C* **2017,** *121* (21), 11368-11379.
9. Gurudayal; Bullock, J.; Sranko, D. F.; Towle, C. M.; Lum, Y.; Hettick, M.; Scott, M. C.; Javey, A.; Ager, J., Efficient solar-driven electrochemical CO_2 reduction to hydrocarbons and oxygenates. *Energy Environ. Sci.* **2017,** *10* (10), 2222-2230.
10. Lee, S.; Park, G.; Lee, J., Importance of Ag–Cu Biphasic Boundaries for Selective Electrochemical Reduction of CO_2 to Ethanol. *ACS Catal.* **2017,** *7* (12), 8594-8604.
11. Hoang, T. T. H.; Verma, S.; Ma, S.; Fister, T. T.; Timoshenko, J.; Frenkel, A. I.; Kenis, P. J. A.; Gewirth, A. A., Nanoporous Copper–Silver Alloys by Additive-Controlled Electrodeposition for the Selective Electroreduction of CO_2 to Ethylene and Ethanol. *J. Am. Chem. Soc.* **2018,** *140* (17), 5791-5797.
12. Gao, J.; Ren, D.; Guo, X.; Zakeeruddin, S. M.; Grätzel, M., Sequential Catalysis Enables Enhanced C-C Coupling towards Multicarbon Alkenes and Alcohols in Carbon Dioxide Reduction: A Study on CuAu Electrocatalysts. *Faraday Discuss.* **2019,** *215*, 282-296.

13. Yano, H.; Tanaka, T.; Nakayama, M.; Ogura, K., Selective Electrochemical Reduction of CO_2 to Ethylene at a Three-phase Interface on Copper (I) Halide-Confined Cu-mesh Electrodes in Acidic Solutions of Potassium Halides. *J. Electroanal. Chem.* **2004,** *565* (2), 287-293.
14. Hsieh, Y.-C.; Senanayake, S. D.; Zhang, Y.; Xu, W.; Polyansky, D. E., Effect of chloride anions on the synthesis and enhanced catalytic activity of silver nanocoral electrodes for CO_2 electroreduction. *ACS Catal.* **2015,** *5* (9), 5349-5356.
15. Schreier, M.; Héroguel, F.; Steier, L.; Ahmad, S.; Luterbacher, J. S.; Mayer, M. T.; Luo, J.; Grätzel, M., Solar conversion of CO_2 to CO using Earth-abundant electrocatalysts prepared by atomic layer modification of CuO. *Nat. Energy* **2017,** *2*, 17087.
16. Schreier, M.; Curvat, L.; Giordano, F.; Steier, L.; Abate, A.; Zakeeruddin, S. M.; Luo, J.; Mayer, M. T.; Grätzel, M., Efficient Photosynthesis of Carbon Monoxide from CO_2 Using Perovskite Photovoltaics. *Nat. Commun.* **2015,** *6*, 7326.
17. Asadi, M.; Kim, K.; Liu, C.; Addepalli, A. V.; Abbasi, P.; Yasaei, P.; Phillips, P.; Behranginia, A.; Cerrato, J. M.; Haasch, R., Nanostructured Transition Metal Dichalcogenide Electrocatalysts for CO_2 Reduction in Ionic Liquid. *Science* **2016,** *353* (6298), 467-470.
18. Zhou, X.; Liu, R.; Sun, K.; Chen, Y.; Verlage, E.; Francis, S. A.; Lewis, N. S.; Xiang, C., Solar-Driven Reduction of 1 atm of CO_2 to Formate at 10% Energy-Conversion Efficiency by Use of a TiO_2-Protected III–V Tandem Photoanode in Conjunction with a Bipolar Membrane and a Pd/C Cathode. *ACS Energy Lett.* **2016,** *1* (4), 764-770.
19. Arai, T.; Sato, S.; Morikawa, T., A Monolithic Device for CO_2 Photoreduction to Generate Liquid Organic Substances in a Single-Compartment Reactor. *Energy Environ. Sci.* **2015,** *8* (7), 1998-2002.
20. Ren, D.; Loo, N. W. X.; Gong, L.; Yeo, B. S., Continuous Production of Ethylene from Carbon Dioxide and Water Using Intermittent Sunlight. *ACS Sustainable Chem. Eng.* **2017,** *5* (10), 9191-9199.
21. Huan, T. N.; Dalla Corte, D. A.; Lamaison, S.; Karapinar, D.; Lutz, L.; Menguy, N.; Foldyna, M.; Turren-Cruz, S. H.; Hagfeldt, A.; Bella, F.; Fontecave, M.; Mougel, V., Low-cost high-efficiency system for solar-driven conversion of CO_2 to hydrocarbons. *Proc. Natl. Acad. Sci. U. S. A.* **2019,** *116* (20), 9735-9740.